Improving microseismic event location accuracy with head wave arrival time: Case study using Marcellus shale

Zhishuai Zhang, James W. Rector, and Michael J. Nava, University of California, Berkeley*

Summary

In this paper, we show that the location of microseismic events can be significantly improved by incorporating information on head wave arrival time. The traditional method of using direct arrival times and P-wave polarizations leads to increased error due to the large uncertainty in polarization. We integrated head wave arrival time to P- and S-wave arrival time to achieve better resolution in microseismic event location. To this end, we developed a Bayesian inference framework for joint event location and velocity model calibration. The developed method was applied for both microseismic event as well as perforation shot location in a project in Marcellus shale. Comparison with location results provided by contractor shows that the developed method can effectively improve the accuracy of microseismic event location. Based on the improvement, we propose a new acquisition geometry and strategy to reduce microseismic monitoring cost and improve event location accuracy.

Introduction

Microseismic processing involves basic location, moment magnitude estimation, and advanced source parameter and frequency analysis (Cipolla et al., 2012; Eisner et al., 2007; Maxwell, 2009, 2014; Warpinski, 2009). The event location, as the basis of almost all other advanced processing, has been routinely conducted by industry. For horizontal wells in shale gas production, it is a common case to have only one nearby well available for microseismic monitoring. Due to the limited azimuthal coverage of acquisition geometry in single horizontal monitor well, microseismic event location with only P- and S-wave arrival time is impossible. An additional constraint on the event location usually comes from direct P-wave polarization (Dreger et al., 1998; Li et al., 2014). However, the unknown orientation of downhole geophones and poor coupling (Gaiser et al., 1988) between geophone and borehole are the challenges to use three component data. These problems, as well as the complexity and anisotropy of shale formation, make the uncertainty in the P-wave polarization significantly large.

Due to shale's low velocity nature, head wave is very common in crosswell seismic (Dong and Toksöz, 1995; Parra et al., 2002; Parra et al., 2006) and microseismic survey (Maxwell, 2010; Zimmer, 2010; Zimmer, 2011) in shale operation. When the distance between geophones and source is relatively large, the head wave arrival can precede direct arrival. Microseismic industry has realized the presence of head wave before direct arrival. Because of its weakness, head wave has been commonly regarded as the contamination of direct arrival. Some preliminary research on making use of head wave has been conducted but mainly on synthetic example of simplified situations (Zimmer, 2010; Zimmer, 2011).

As an inverse problem, the microseismic event location in downhole monitoring can be carried out in various ways. Commonly used methods include least-square travel time inversion (Douglas, 1967; Li et al., 2014), double-difference (Waldhauser and Ellsworth, 2000), coherence scanning (Drew et al., 2005; Duncan and Eisner, 2010), full-waveform inversion. Through effective to a certain extent, these methods don't follow a rigorous statistical framework. The Bayesian inversion (Tarantola, 2005; Tarantola and Valette, 1982) has been used for earthquake (Myers et al., 2007; Myers et al., 2009) as well as microseismic event location (Poliannikov et al., 2014). It has been shown to be an effective tool for joint inversion and uncertainty analysis. However, further work is needed to make full use of this method.

We applied the Bayesian inversion for microseismic event location as well as velocity model calibration. Our event location result on microseismic survey conducted on a single horizontal monitor well in Marcellus shale shows that head wave conveys very useful information. Thus, it can be used to eliminate the requirement for P-wave polarization to improve microseismic event location accuracy.

Theory and Method

Head wave

Head wave is common in microseismic survey in shale (Maxwell, 2010; Zimmer, 2010; Zimmer, 2011). The existence of head wave in Marcellus shale can be shown by the simple yet common configuration in Figure 1. When the angle of incidence equals the critical angle, $\arcsin(V_1/V_2)$, there will be head wave that travels along the interface at the speed of the high velocity layer.

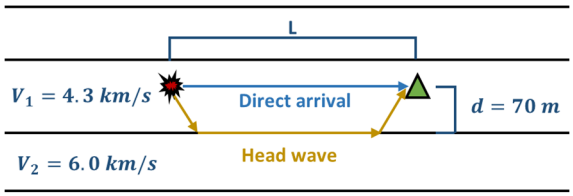

Figure 1: A common configuration for head wave in shale gas operation. Due to the low velocity nature of shale, headwave is common when there is a nearby high velocity layer.

DOI http://dx.doi.org/10.1190/segam2015-5919420.1

Head wave amplitude decays to be inversely proportional to the square of travel distance while body wave amplitude decays to be inversely proportional to the distance. As such, head wave amplitude is usually low, thus difficult to be identified when it appears after the high amplitude direct arrival. However, as its name implies, head wave is typically faster and arrives ahead of other waves. Figure 2 shows that the head wave can take over direct arrival to be the first arrival after the cross-over distance.

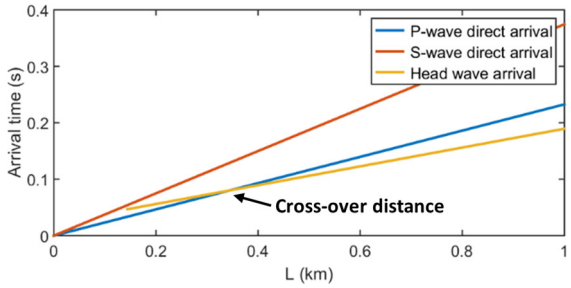

Figure 2: Arrival time of various phases as a function of source receiver distance. When source receiver distance is larger than the cross-over distance, head wave can overtake direct arrival to be the first arrival.

Due to its low amplitude, head wave has been regarded as the contamination of direct arrival, especially when it arrives before direct P arrival. However, our study shows that head wave is actually a valuable source of information that should be not dismissed since its travel path covers a larger area than the direct arrival path.

Bayesian inversion for microseismic event location

To estimate the microseismic event location within a rigorous statistical framework, we applied the Bayesian inversion for microseismic event location. From inverse problem theory (Tarantola, 2005; Tarantola and Valette, 1982), we can demonstrate that under Gaussian assumption, the a posteriori information of the model can be given by:

$$\sigma_{\mathbf{M}}(\mathbf{m}) \propto \exp\left\{-\frac{1}{2}\left[(\mathbf{g}(\mathbf{m})-\mathbf{d_{obs}})^T\mathbf{C_D^{-1}}(\mathbf{g}(\mathbf{m})-\mathbf{d_{obs}}) + (\mathbf{m}-\mathbf{m_{prior}})^T\mathbf{C_m^{-1}}(\mathbf{m}-\mathbf{m_{prior}})\right]\right\}$$

where $\mathbf{d_{obs}}$ is a vector containing the observed data. In the problem of microseismic event location, it can be an array of arrival times of all identifiable phases, and the polarization information if desired. The data covariance matrix $\mathbf{C_D} = \mathbf{C_d} + \mathbf{C_T}$ is the sum of the observation part $\mathbf{C_d}$ and model part $\mathbf{C_T}$. The model parameter vector $\mathbf{m}$, and its prior information $\mathbf{m_{prior}}$ contain the spacial coordinate and origin time of microseismic events. The parameters describing velocity model can also be a part of the model parameter if we want to do a joint inversion of event locations and velocity model. $\mathbf{C_m}$ is the parameter covariance matrix of the prior information. The forward operator $\mathbf{g(m)}$ is a function of the model parameters $\mathbf{m}$ and will give a prediction on the observable data $\mathbf{d}$ based on the model parameters. We use a ray tracing method as the forward operator to predict the arrival time based on event location and origin time.

The solution to the posterior probability density function (PDF) of model parameter can be challenging (Oliver et al., 2008; Tarantola, 2005). Here, we adopted a Maximum A Posteriori (MAP) estimation (Oliver et al., 2008; Zhang et al., 2014) to characterize the posterior PDF of microseismic event location and origin time. The MAP estimation method tries to find the peak of the posterior PDF and regards the model at this point as the most likely case given the prior information and observation. This can be accomplished by minimizing the exponent of the posteriori probability density with a Gauss-Newton method (Zhang et al., 2014).

Microseismic Survey Overview

The hydraulic fracturing was performed in the Marcellus formation in Susquehanna County, Pennsylvania, within Susquehanna River Basin. Two horizontal wells were drilled as shown by Figure 3. The length of the horizontal portion of the monitor and stimulation well are 1.35 and 1.7 km respectively. Average distance between the horizontal portions of the two wells is around 0.22 km.

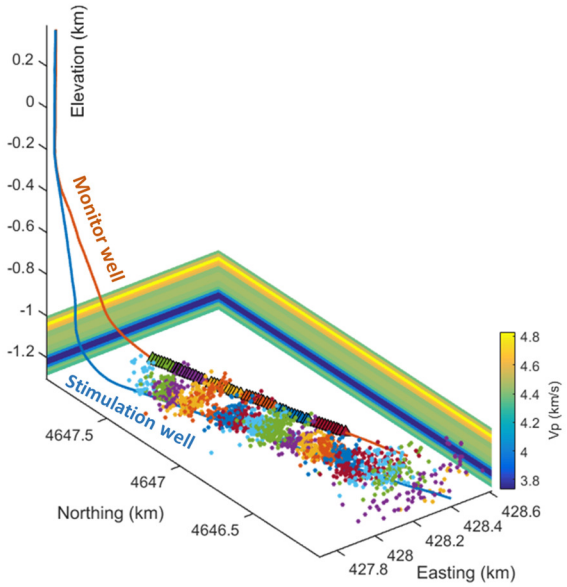

Figure 3: Microseismic survey geometry. The microseismic event location (dots) were processed by contractor. The geophone array is colored according to their locations. Microseismic events are colored according to their associated stimulation stages.

Eighteen hydraulic fracturing stages were conducted with four perforation shots prior to each stimulation stage (Figure 4). Microseismic monitoring was carried out with an array of eleven three-component geophones. The geophone

DOI http://dx.doi.org/10.1190/segam2015-5919420.1

spacing in the array is approximately 15 m. The array was moved according to the location of hydraulic fracturing stages to minimize the noise due to source receiver distance. The contractor-estimated locations of microseismic events are also shown on Figure 3.

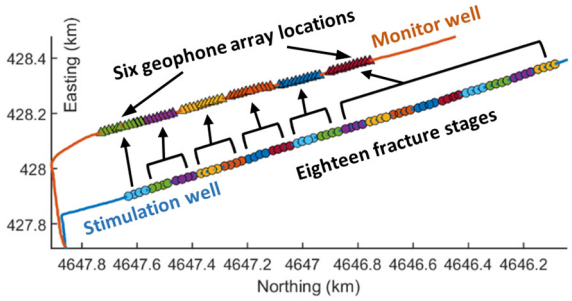

Figure 4: The stimulation was performed in 18 stages and the microseimsic signal was recorded by an array of 11 geophoens in the nearby monitoring well. The geophone array was moved according to the stimuation stage location to reduce the error due to large observaton distance.

In addition to these microseismic events, most of the perforation shots were recorded by the geophone array and can be used for velocity model calibration and location uncertainty analysis.

Observation of Head Wave

Head wave is commonly observed in waveforms of both perforation shots and microseismic events, especially those in the early fracking stages given their relatively large distance from the monitoring geophone array. Figure 5 is a typical set of waveforms and moveout recorded by the geophone array. We can easily identify the head wave arrival based on its low amplitude and high velocity moveout.

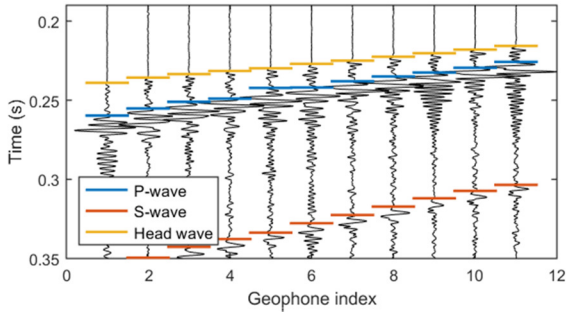

Figure 5: The waveform of a perforation shot recorded by an array of geophones. Head wave can be easily identified based on their low amplitude and high velocity moveout.

To further verify and analyze the head wave, the finite difference simulation of microseismic wave propagation in the configuration of this project was conducted by Lawrence Livermore National Laboratory's SW4 code (Petersson and Sjogreen, 2013). The existence of head wave can be verified by the comparison between real and synthetic waveform as shown by Figure 6. Both the amplitude and arrival time of head wave in real data match the synthetic waveform well.

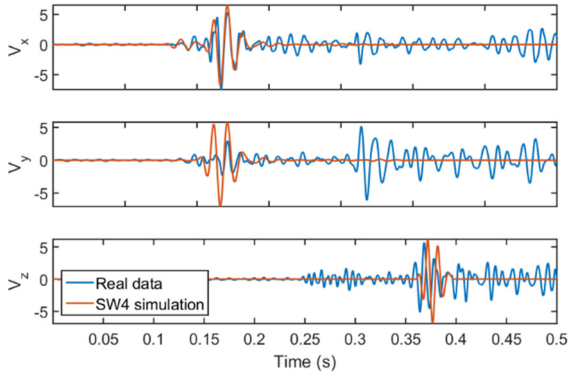

Figure 6: Comparison between synthetic and real waveform. The synthetic waveform matches the real data relatively well. This verified the existence of head wave. The difference on S-wave in x and y components may be because of the unknown source mechanism of the real event for simulation.

Results and Discussion

Velocity model calibration

The original velocity model used by the contractor as shown in Figure 3 was isotropic layered model built based on sonic logs. However, analysis on this velocity model shows that head wave will not take over direct arrival to be the first arrival in this configuration. So the velocity model will need to be calibrated to waveform of perforation shots. This can be carried out by our developed Bayesian inversion code for microseismic event location. We can simply use the velocity model as the model parameter **m** and perforation shot location as the observable data **d**. From the velocity model calibration, we found the stimulation zone can be precisely characterized by the original velocity model ($V_p = 4.31\ km/s$ and $V_s = 2.67\ km/s$). However, the calibration also reveals the existence of a high velocity ($V_p = 6.01\ km/s$) zone approximately 70 m below the geophone array but there was no velocity information in the original model due to lack of sonic log.

Perforation shot location

To quantify our event location estimation accuracy, we located the perforation shots whose locations are known. Our location result of the four perforation shots on stage two, along with their true location, is shown by Figure 7. What is also shown is the location result with the traditional method, which used direct arrivals and P-wave polarization. Before the location of perforation shots in this analysis, the velocity model was calibrated with all available perforation shots on

DOI http://dx.doi.org/10.1190/segam2015-5919420.1

stages other than stage two. Since the velocity model was not calibrated with perforation shots to be located, these perforation shots on stage two can be treated as normal microseismic events and used for location uncertainty analysis.

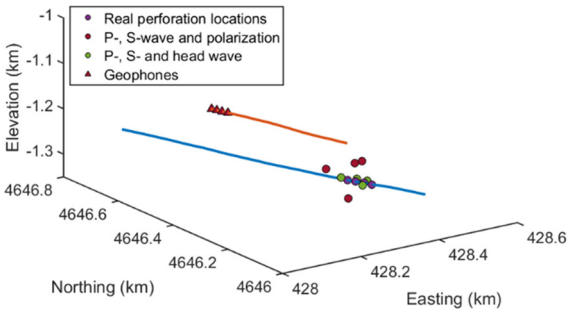

Figure 7: Comparison on estimated perforation shots location and the true perforation location. The perforation shot location estimated with P-, S-, and head waves is very accurate.

From the comparison we found the method using head wave gives an average error of 15 m while the traditional method with polarization gives an error of 49 m. This demonstrates the effectiveness and accuracy of our proposed location method with head wave arrival time.

Relocation of microseismic events on stage two

The map view of the microseismic event location provided by the contractor is shown in Figure 8. Apparently, the microseismic event location on stages two is significantly more scattered than those on later stages. One possible explanation of the scattering is because of the larger stimulated reservoir volume for stage two. Another explanation is simply because of the large location uncertainty due to the long distance of stage two from the geophone array.

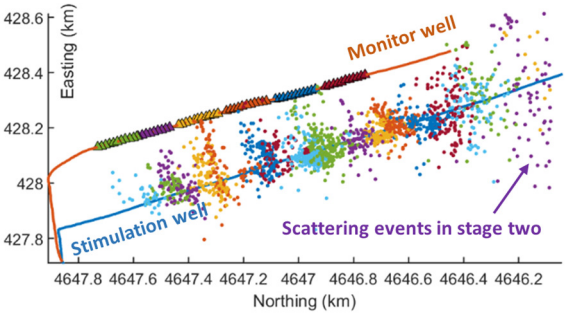

Figure 8: Map view of microseismic event location processed by contractor. The event location on stage two is more scattered than those in later stages.

To find the reason for the scattering of stage two events, we relocated these events with head wave arrival as a substitution for polarization as shown in Figure 9. The relocated events are much less scattered than the result provided by contractor. This shows that the scattering of stage two events in original catalog was due to the large uncertainty in the estimation. Also, it indicates the effectiveness of accounting for head wave in microseismic event location to improve location accuracy.

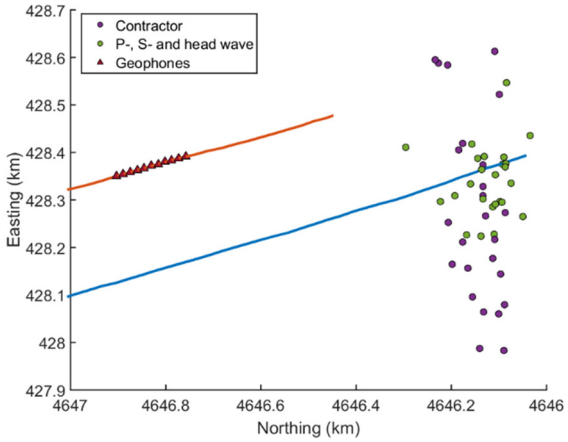

Figure 9: The microseismic event location estimated with P, S and head wave arrival is less scattered when compared to the microseismic event location processed by the contractor.

Since it is difficult to pick head wave that arrives after direct P-wave arrival, we will be forced to use polarization to constrain the event location near the geophones. This traditional method is problematic as we have shown. We would propose a two-array geophones acquisition geometry for single horizontal well monitoring. One array should be as near to the stimulation zone as possible. And the other array should be at relatively large distance from the stimulation zone for head wave monitoring. This acquisition geometry will be able to use head wave arrivals as well as obtain high S/N ratio.

Conclusion

The existence of head wave in microseismic survey in Marcellus shale is observed and verified. A Bayesian inversion framework was developed for microseismic event location and velocity model calibration. The location result of perforation shots using the developed method verified that the accounting for head wave arrival time as a substitution of P-wave polarization indeed improves the microseismic location accuracy. The relocation result on microseismic events in stage two shows a more reasonable pattern than the original catalog. Based on the developed method, we proposed a new acquisition geometry for single horizontal well hydraulic fracturing monitoring, which enables us to improve microseismic event location accuracy.

DOI http://dx.doi.org/10.1190/segam2015-5919420.1

EDITED REFERENCES

Note: This reference list is a copyedited version of the reference list submitted by the author. Reference lists for the 2015 SEG Technical Program Expanded Abstracts have been copyedited so that references provided with the online metadata for each paper will achieve a high degree of linking to cited sources that appear on the Web.

REFERENCES

Cipolla, C., S. Maxwell, M. Mack, and R. Downie. 2012, A practical guide to interpreting microseismic measurements: SPE/EAGE European Unconventional Resources Conference and Exhibition — From Potential to Production.

Dong, W., and M. N. Toksöz, 1995, Borehole seismic-source radiation in layered isotropic and anisotropic media: Real data analysis: Geophysics, **60**, 748–757. http://dx.doi.org/10.1190/1.1443813.

Douglas, A., 1967, Joint epicenter determination: Nature, **215**, no. 5096, 47–48. http://dx.doi.org/10.1038/215047a0.

Dreger, D., R. Uhrhammer, M. Pasyanos, J. Franck, and B. Romanowicz, 1998, Regional and far-regional earthquake locations and source parameters using sparse broadband networks: A test on the Ridgecrest sequence: Bulletin of the Seismological Society of America, **88**, no. 6, 1353–1362.

Drew, J. E., H. D. Leslie, P. N. Armstrong, and G. Michard, 2005, Automated microseismic event detection and location by continuous spatial mapping: SPE Annual Technical Conference and Exhibition. http://dx.doi.org/10.2118/95513-MS.

Duncan, P., and L. Eisner, 2010, Reservoir characterization using surface microseismic monitoring: Geophysics, **75**, no. 5, 75A139–75A146. http://dx.doi.org/10.1190/1.3467760.

Eisner, L., and J. H. Le Calvez, 2007, New analytical techniques to help improve our understanding of hydraulically induced microseismicity and fracture propagation: Presented at the SPE Annual Technical Conference and Exhibition, http://dx.doi.org/10.2118/110813-MS.

Gaiser, J. E., T. J. Fulp, S. G. Petermann, and G. M. Karner, 1988, Vertical seismic profile sonde coupling: Geophysics, **53**, 206–214. http://dx.doi.org/10.1190/1.1442456.

Li, J., C. Li, S. A. Morton, T. Dohmen, K. Katahara, and M. Nafi Toksöz, 2014, Microseismic joint location and anisotropic velocity inversion for hydraulic fracturing in a tight Bakken reservoir: Geophysics, **79**, no. 5, C111–C122. http://dx.doi.org/10.1190/geo2013-0345.1.

Maxwell, S., 2009, Microseismic location uncertainty: CSEG Recorder, April.

Maxwell, S., 2010, Microseismic: Growth born from success: The Leading Edge, **29**, 338–343. http://dx.doi.org/10.1190/1.3353732.

Maxwell, S., 2014, Microseismic imaging of hydraulic fracturing: Improved engineering of unconventional shale reservoirs: SEG, no. 17. http://dx.doi.org/10.1190/1.9781560803164.

Myers, S. C., G. Johannesson, and W. Hanley, 2007, A Bayesian hierarchical method for multiple-event seismic location: Geophysical Journal International, **171**, no. 3, 1049–1063. http://dx.doi.org/10.1111/j.1365-246X.2007.03555.x.

Myers, S. C., G. Johannesson, and W. Hanley, 2009, Incorporation of probabilistic seismic phase labels into a Bayesian multiple-event seismic locator: Geophysical Journal International, **177**, no. 1, 193–204. http://dx.doi.org/10.1111/j.1365-246X.2008.04070.x.

Oliver, D. S., A. C. Reynolds, and N. Liu, 2008, Inverse theory for petroleum reservoir characterization and history matching: Cambridge University Press. http://dx.doi.org/10.1017/CBO9780511535642.

Parra, J. O., C. L. Hackert, A. W. Gorody, and V. Korneev, 2002, Detection of guided waves between gas wells for reservoir characterization: Geophysics, **67**, 38–49. http://dx.doi.org/10.1190/1.1451322.

Parra, J. O., C. L. Hackert, P.-C. Xu, and H. A. Collier, 2006, Attenuation analysis of acoustic waveforms in a borehole intercepted by a sand-shale sequence reservoir: The Leading Edge, **25**, 186–193. http://dx.doi.org/10.1190/1.2172311.

Petersson, N. A., and B. Sjogreen, 2013, User's guide to SW4, version 1.0, *in* LLNL-SM-xxyy: Lawrence Livermore National Laboratory.

Poliannikov, O. V., M. Prange, A. E. Malcolm, and H. Djikpesse, 2014, Joint location of microseismic events in the presence of velocity uncertainty: Geophysics, **79**, no. 6, KS51–KS60. http://dx.doi.org/10.1190/geo2013-0390.1.

Tarantola, A., and B. Valette, 1982, Inverse problems = quest for information: Journal of Geophysics, **50**, 150–170.

Tarantola, A., 2005, Inverse problem theory and methods for model parameter estimation: SIAM.

Waldhauser, F., and W. L. Ellsworth, 2000, A double-difference earthquake location algorithm: Method and application to the northern Hayward fault, California: Bulletin of the Seismological Society of America, **90**, no. 6, 1353–1368. http://dx.doi.org/10.1785/0120000006.

Warpinski, N., 2009, Microseismic monitoring: Inside and out: Journal of Petroleum Technology, **61**, no. 11, 80–85. http://dx.doi.org/10.2118/118537-JPT.

Zhang, Z., B. Jafarpour, and L. Li, 2014, Inference of permeability heterogeneity from joint inversion of transient flow and temperature data: Water Resources Research, **50**, no. 6, 4710–4725. http://dx.doi.org/10.1002/2013WR013801.

Zimmer, U., 2010, Localization of microseismic events using headwaves and direct waves: Presented at the 80th Annual International Meeting, SEG. http://dx.doi.org/10.1190/1.3513282.

Zimmer, U., 2011, Microseismic design studies: Geophysics, **76**, no. 6, WC17–WC25. http://dx.doi.org/10.1190/geo2011-0004.1.